Proceedings of the ASME 2017 12th International Manufacturing Science and Engineering Conference
MSEC2017
June 4-8, 2017, Los Angeles, CA, USA

MSEC2017-3034

Simulations of Microstructure Evolution during Friction Stir Blind Riveting using a Cellular Automaton Method

Avik Samanta[1], Ninggang Shen[1], Haipeng Ji[1,2], Weiming Wang[3], Hongtao Ding[1]*, Jingjing Li[4]

[1] Department of Mechanical and Industrial Engineering, University of Iowa, Iowa City, IA 52242, USA
[2] Research Institute for Energy Equipment Materials, Hebei University of Technology, Tianjin, 300130, China
[3] Department of Mechanical Engineering, University of Hawaii at Manoa, Honolulu, HI 96822
[4] The Harold and Inge Marcus Department of Industrial and Manufacturing Engineering, Penn State University, State College, PA 16801, USA

KEYWORDS
Cellular Automaton; Friction stir blind riveting; Modeling; Microstructure evolution; Dynamic recrystallization.

ABSTRACT

Friction stir blind riveting (FSBR) is a novel and highly efficient joining technique for lightweight metal materials, such as aluminum alloys. The FSBR process induced large gradients of plastic deformation near the rivet hole surface and resulted in a distinctive gradient microstructure in this domain. In this study, microstructural analysis is conducted to analyze the final microstructure after the FSBR process. Dynamic recrystallization (DRX) is determined as the dominant microstructure evolution mechanism due to the significant heat generation during the process. To better understand the FSBR process, a two-dimensional Cellular Automaton (CA) model is developed to simulate the microstructure evolution near the rivet hole surface by considering the FSBR process loading condition. To model the significant microstructure change near the rivet hole surface, spatial distributed temporal thermal and mechanical loading conditions are applied to simulate the effect of the large gradient plastic deformation near the hole surface. The distribution grain topography and recrystallization fraction are obtained through the simulations, which agree well with the experimental data. This study presents a reliable numerical approach to model and simulate microstructure evolution governed by DRX under the large plastic deformation gradient in FSBR.

1. INTRODUCTION

In transportation industries, the reduction of effective weight of the moving masses without compromising the safety is one of the key challenge for next generation vehicles. Aluminum alloys have been widely used as light metal in automobile industries especially in vehicle bodies to reduce its effective weight leading to improvement in fuel economy and reduction in CO_2 emission. Some of this light metals are difficult to join by conventional spot welding process, so considerable amount of research is going on to develop new joining process to join sheet metal quickly and economically.

Wang and Stevenson [1,2] invented the friction stir blind riveting (FSBR) process by combining friction stir and blind riveting processes. During the FSBR process, a high speed rotating (2000~12000 rpm) blind rivet is brought in contact with the upper sheet of a stack of sheet metals. The stack can be a collection of 2~4 sheet metal in lap joint configuration. The frictional heat generated between rivet and workpiece softens the material leading to reduction of required force to drive the rivets into the workpiece. When the rivet is fully inserted into the workpiece, it is upset as in conventional blind riveting.

The performance of the mechanical joint by FSBR process has been considerately studied for joining similar and dissimilar materials [2–7] in recent years. Gao et. al [2] first conducted experimental analysis of FSBR process on Aluminum alloys and proved this process is able to provide better static and fatigue strength compared to other joining processes. Later Min et al [4] studied the effect of process parameters like spindle speed and feed rate on penetration force/torque and consumed energy during frictional penetration of blind rivets into Aluminum

*Corresponding author: hongtao-ding@uiowa.edu, +1-319-335-5674

sheets. Increase in feed rate significantly increase the penetration force while increase in spindle speed reduce the penetration force due to more thermal softening of material at higher rotational interaction of the mandrel with the material. Min et al [5,6] investigated the FSBR process to join dissimilar materials Magnesium and Aluminum alloy which are very difficult to weld together. The placement of the sheets also plays a significant role for joint strength. They also found that the material around the rivet shank get hardened during the penetration process which significantly affect the joint strength. Later, Min et al used the FSBR process to join carbon-fiber reinforced polymer composites to aluminum alloy. The joint strength depends on the track-up sequence of the sheets [7].

In recent years, Cellular Automata (CA) method has been developed to simulate the microstructure evolution governed by dynamic recrystallization (DRX) during the hot deformation processes of various metals, e.g. carbon and alloy steels [8–15], copper [16–21], magnesium alloys [22–24], and titanium alloy [25,26]. These previous work demonstrated that the CA method is an efficient approach to predict the microstructure evolution with reasonable computational cost. However, all the previous work focused on the hot deformation processes with low strain rate and usually under constant thermal loadings.

To better understand the FSBR process, a two-dimensional (2D) CA approach is implemented for a quantitative and topographic prediction of the microstructure evolution under the large gradient of plastic deformation in the process. The large gradient of plastic deformation is modeled by applying spatial distributed temporal thermal and mechanical loading conditions. The distribution and history of grain topography and recrystallization fraction are obtained. The simulated grain size distributions agree well with the experimental data, so the developed CA model is validated. This model is a reliable numerical approach for predicting microstructure evolution governed by DRX under the large plastic deformation gradient.

2. EXPERIMENTS OF FSBR

The principle of Friction stir riveting process is based on the experimental work conducted by Min et al. [27]. Table 1 shows the details of the experimental conditions. In the experimental study of FSBR process, an AA6111-T4 sheet with a gage thickness of 0.9 mm, is penetrated by FSBR process. The experiment is conducted by using blind rivets SSPV-08-06 manufactured by Advel®, USA with shank diameter 6.4 mm. The rivets are made of mild steel and it has a fine zinc coating on the surface. Table 2 lists down physical and mechanical properties of the workpiece and rivets.

Table 1: Experimental Conditions [27].

Materials	AA 6111-T4(Sheets) Zinc coated Mild-Steel (Rivets)
Sheet Thickness	0.9 mm
Rotational speed	6000 rpm
Feed rate	780 mm/min

The AA6111-T4 sheet was rolled and annealed before the experiment and it had strain free equiaxed grains as shown in Fig. 1a. The average grain size was 24.9 ± 1.9 µm. After the FSBR process, the specimen was sectioned along the rivet axis and polished in Struers polishing machine. Then, the specimen is etched with 0.5% HF for 3 seconds followed by the standard EBSD analysis using CARL ZEISS scanning electron microscope. Three different analysis step sizes are used for the analysis. Fine step size of 1µm is used near the hole surface and gradually it is increased to 3 µm away from the hole surface. Fig.

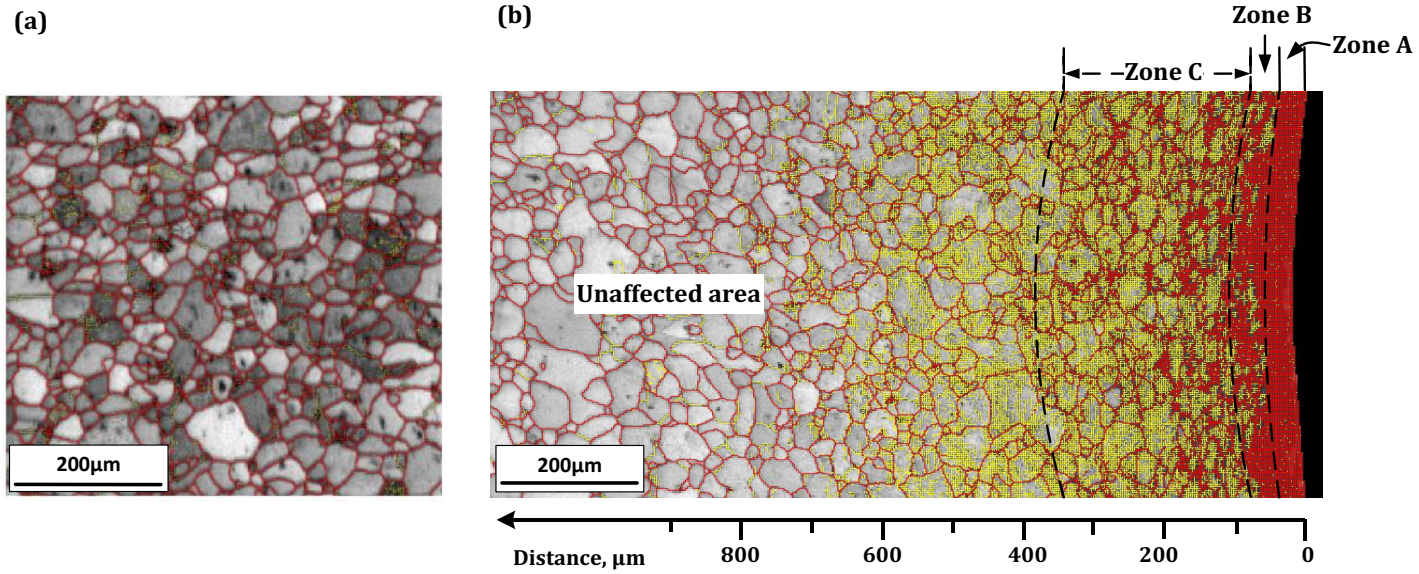

Fig. 1: Microstructure evolution in the rivet wall: a) equiaxed original microstructure; b) classification of different zones based on the grain evolution after the process (original images adopted from [27]).

1b shows the microstructure of the specimen processed with experimental condition mentioned in Table 1. Average grain size was calculated by analyzing the micrograph using open source MATLAB program "linecut". Significant grain size refinement was observed near the friction stir penetrated hole surface after the process (Fig. 1b). The average grain size in different zones is shown in Fig. 2. The grain size was as low as 1~2 μm near the hole surface and gradually increased away from the hole surface. Beyond 350μm the average grain size was similar to as received material.

Table 2: Mechanical and Physical Properties[28,29]

Property	AA6111-T4	Steel (rivet)
Density (kg/m^3)	2710	7800
Young's modulus (GPa)	70	200
Poisson's ratio	0.33	0.30
Yield Strength (MPa)	165	386
Thermal conductivity (W/m·°C)	167	47.7
Heat Capacity (J/Kg.°C)	996	432.6

The evolution of microstructure as shown in Fig. 1-3 highly depends on the process temperature and shear deformation in the domain. FSBR process involve sliding and sticking contact between rivet and workpiece material as in all friction stir processes [30]. When the high speed rotating rivet penetrate into the workpiece, workpiece material closest to the hole partially stuck with the rivet surface and stirred during the process. As a result, the material undergoes severe plastic deformation near the hole surface. This region also has higher process temperature as

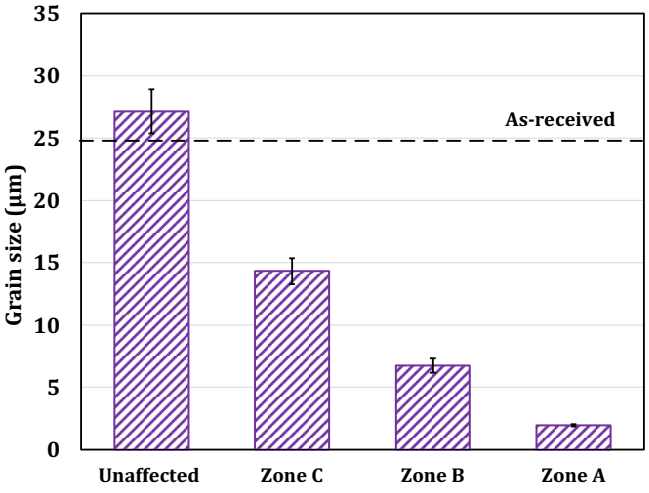

Fig. 2: Grain size Measurement

it is very close to the frictional heat flux between base material and rivet. It is most likely that the temperature in this region reaches up to the recrystallization temperature range. Severe shear deformation also indicates that it should have stored enough strain energy to trigger the dynamic recrystallization (DRX) [31–33]. At the same time, if the material underwent severe plastic deformation, there is higher rate of nucleation compare to the rate of growth [34]. On the contrary, as we move away from the hole surface, less plastic deformation happens as the stirring effect reduces as distance increases. It also has low temperature as they are far from the frictional heat source. As the temperature at the surrounding is still very low, the temperature drops immediately after the completion of the process. These two reason might have prevented to have grain growth after the DRX.

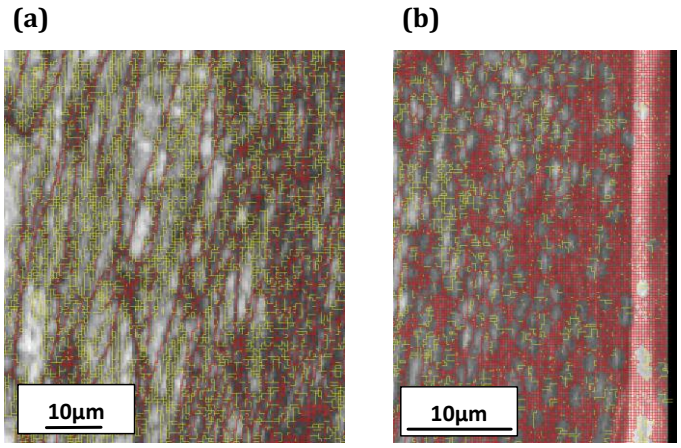

Fig. 3: Zoom in view of the (a) zone B and (b) zone A

Based on the above analysis, the microstructural evolution during the FSBR process is significantly important as it explains the existence of fine recrystallized grains near the penetrated hole surface and coarse grains as you go away from the hole edge. The final microstructure is determined by a 2D model based on CA method to understand the evolution of grins during this process.

3. CELLULAR AUTOMATON MODEL

Dynamic recrystallization (DRX) has a significant effect on the evolution of microstructure during manufacturing processes as they are dominated by high shear deformation and temperature gradient resulting in grain refinement to improve strength and toughness. Therefore, it is very important to understand the mechanism and predict the dynamic recrystallized microstructures to control the mechanical properties of end product. So far, there have been a lot of researches on dynamic recrystallization in manufacturing processes, but mainly focus on macroscopic experiments and finite element simulation. It is difficult to directly observe the dynamic process of microstructure evolution during DRX. The development of cellular automata technique has provided the possibility for simulating and predicting the evolution of microstructure during manufacturing processes dominated by high gradient thermal and mechanical loading. In this study, a MATLAB code is developed based on cellular automata technique.

3.1 Model Assumptions

It has been widely studied that DRX is triggered when the dislocation density reaches a critical value in a deformed material. This critical value depends on two important processing parameters as temperature and strain rate distribution in the analysis domain [21,35]. Two important features during dynamic recrystallization are nucleation and grain growth. Both of them are greatly influenced by the evolution of dislocation density inside a grain. In order to simplify the CA model this article considers the following five basic assumptions:

(1) To simplify the structure, grain rotation is ignored which means there is no texture in the deformation of the grains. It is also considered that there is no existence of vacancy, twins, stacking fault, the second phase particles and other defects in the crystal.

(2) AA6111 alloy used for the FSBR experiment is in T4 condition which is solutionized and natural aging condition. The dislocation density in a well annealed aluminum is in the range of 10^{10} /m^2 [36,37]. It is assumed that the initial dislocation density is uniform and equal in the initial grains. At the onset of DRX, nucleation of a new grain happens at the grain boundary. It is assumed that the new grain is dislocation free. For the recrystallized grains, the dislocation density is reset to a very low number and it further evolves based on the strain rate and temperature distribution in the domain.

(3) Recrystallization grain nucleation happens only at the grain boundary which includes primary grain boundary and recrystallized grain boundary. This assumption is based on the several experimental observation about bulk nucleation at grain boundaries [38,39]

(4) Only the dislocation density and grain boundary energy is considered as the driving force of recrystallization simulation. Effect of elastic strain energy, surface energy is ignored.

(5) When the dynamic recrystallization grain dislocation density reaches the critical dislocation density, nucleation of a new dynamic recrystallized grain occurs at the grain boundary.

3.2 Modeling of Dislocation Evolution

During the deformation process, dislocation density is evolved according to work hardening and dynamic recovery (softening). The mean dislocation density is calculated as the sum of both of these competing processes:

$$\frac{\partial \rho}{\partial \varepsilon} = \left(\frac{\partial \rho}{\partial \varepsilon}\right)_{hard} + \left(\frac{\partial \rho}{\partial \varepsilon}\right)_{soft} \tag{1}$$

The first term on the right side of the equation is the increase in dislocation density due to work hardening, and the second term is the decrease in dislocation density due to softening associated with dynamic recovery. During the hot deformation of the metal, the work hardening and the softening are always carried out simultaneously. The change of the dislocation density depends on the result of the competition between the two processes.

The change of dislocation density during stage III hardening of metals is modeled based on the phenomenological model (KM model) proposed by Kocks and Mecking [40,41]. This model considers that dislocation density is the single structural parameters that controls the kinetics of plastic flow of materials. The change of the mean dislocation density for different strain can be expressed as mentioned by Estrin [42]

$$\frac{\partial \rho}{\partial \varepsilon} = k_1\sqrt{\rho} + \frac{1}{bd} - k_2\rho \tag{2}$$

where $k1$ is a constant; b is Burger's vector; d is the mean grain size and $k2$ is the softening parameter which is a function of temperature and strain rate, $k2 = f(\dot{\varepsilon},T)$.

For a simulation domain subjected to deformation, the evolution of dislocation is calculated by equation (2). The occurrence of nucleation during DRX is based on the accumulation of dislocations. When the mean dislocation density in the deformed metal reaches the critical dislocation density during thermomechanical process, the nuclei for DRX will start to form on grain boundaries. Stuwe and Ortner [43] proposed a theoretical model to calculate critical dislocation density. The critical dislocation density is used instead of the critical strain to describe the necessary conditions for the dynamic recrystallization. According to Roberts and Ahlblom [44], the value of critical dislocation density determined by the deformation conditions, and it is calculated by the change in energy associated with the formation of a nucleus on a pre-existing grain boundary.

$$\rho_c = \left(\frac{20\gamma_m \dot{\varepsilon}}{3blM\tau^2}\right)^{1/3} \tag{3}$$

where γ_m is the grain boundary energy; l is the dislocation mean free path; M is the grain boundary mobility; τ is the dislocation line energy, and. γ_m, l , M and τ are obtained by the following formulas:

$$\gamma_m = \frac{\mu b\theta_m}{4\pi(1-\nu)} \tag{4}$$

$$l = \frac{K_1\mu b}{\sigma} \tag{5}$$

$$M = \frac{\delta D_{0b} b}{KT}\exp\left(-\frac{Q_b}{RT}\right) \tag{6}$$

$$\tau = c_2\mu b^2 \tag{7}$$

where; μ is the shear modulus, θ_m is mis-orientation for a high angle boundary here it is assumed as 15°. ν is Poisson's ratio; K_1 is material constant, for most metals it is 10; δ is the grain boundary thickness of the material; K is Boltzmann constant, D_{ob} is grain boundary self-diffusion coefficient at 0K. Q_b is grain boundary diffusion activation energy; R is ideal gas constant and c_2 is material constant.

Table 3: CA model constants for AA 6111[45,46]

b, (nm)	μ (GPa)	Q_b (kJ.mol^{-1})	Q_{act} (kJ.mol^{-1})	δD_{0b} (m^3.s^{-1})	R (J.mol^{-1}K^{-1})	θ_m (rad)
0.286	25.9	82	142	5.0×10^{-14}	8.314	π/12

3.3 Modeling of Nucleation Rate

In this study, nucleation rate is calculated based on the model proposed by Ding and Guo [21] which incorporated the influence of processing temperature of deformation [35] and strain rate [47].

$$\dot{n}(\dot{\varepsilon},T) = C\dot{\varepsilon}^m \exp\left(-\frac{Q_{act}}{RT}\right) \tag{8}$$

where C is constant; $\dot{\varepsilon}$ is the strain rate; exponent m is a constant and its value is 1; Q_{act} is the activation energy; R is Ideal gas constant, and T is temperature in Kelvin.

The DRX percentage is calculated by.

$$\eta = \dot{n}\frac{\varepsilon}{\dot{\varepsilon}}\frac{4}{3}\pi r_d^3 \tag{9}$$

where η is the percentage of DRX, ε is the true strain and r_d is the mean radius of all the recrystallized-grains.

The value of the mean radius of all the recrystallized grains is calculated using:

$$\frac{\sigma_s}{\mu}\left(\frac{2r_d}{b}\right)^n = K \tag{10}$$

Where σ_s is the steady state flow stress, n is a constant and its value is 2/3 and K is a material constant.

3.4 Recrystallized Grain Growth

Dislocation density is the driving force for the nucleation site during growth. The grain boundary tends to move from the side of the recrystallized grains with low dislocation density to the grains with high dislocation density due to the driving force associated with difference in the dislocation density between the matrix grains and the recrystallized grains. For the first recrystallization grain, the growth rate follows the equation:

$$V_i = Mf_i \tag{11}$$

where f_i is the growth driving force per unit area of the recrystallized grains is represented by the following formula:

$$f_i = \tau(\rho_m - \rho_i) - 4\frac{\gamma_i}{d_i} \tag{12}$$

where ρ_m is the dislocation density of matrix grains; ρi is dislocation density of recrystallized grains; di is the diameter of recrystallized grains; γi is the grain boundary energy between the matrix and the recrystallized grains is calculated as follows:

$$\gamma_i = \begin{cases} \gamma_m \frac{\theta_i}{\theta_m}[1-\ln(\frac{\theta_i}{\theta_m})] & for \quad \theta_i \le \theta_m \\ \gamma_m & for \quad \theta_i \le \theta_m \end{cases} \tag{13}$$

where θ_i is the orientation difference between the recrystallized grains i and the adjacent crystal grains. The material parameters used for the CA simulation of AA 6111-T4 is listed in Table 3 [45,46].

3.5 Initial Grain Structure

Before simulating the DRX, the initial microstructure was simulated using a simple grain growth algorithm. The simulation domain is set as 400μm × 200 μm. The step by step procedure is mentioned below:

1. Cell: A square cell of 1.0 μm × 1.0 μm was used.
2. Cell state: The simulation process gives each cell six state control variables, as follows:
   A. Orientation variable: different grains with different orientation number distinction, grain cell orientation values are 1-180, randomly generated.
   B. Dislocation density variable: dislocation density represents the deformation of the grain storage energy. If the dislocation density of the boundary cell reaches the critical dislocation density ρ_c, the cell undergoes nucleation according to the probability of nucleation, and the dynamic recrystallization takes place.
   C. Grain boundary variable: In this model, the two-layer cell at the grain boundary is the grain boundary. To distinguish the grain from the grain boundary, we set the grain boundary variable, which is 0 and 1. Grain boundary cell is 0.
   D. The grain number of variables: each grain has a unique number, for the number of recrystallized grains.
   E. The number of recrystallization variables: the value of an integer, used to measure dynamic recrystallization grain size, recrystallization does not occur the number of cell variables is 0, recrystallization occurs when the number of cell variables plus one.
   F. Color display variables: used to simulate the recrystallization grain morphology features, the parent phase is displayed as black and white graphics, recrystallization grain is displayed as RGB color images.
3. Cell space: In this model, 400 × 200 two-dimensional square cells are used, and the simulated region represents 400 μm × 200 μm real size.
4. Neighbor type: Considering the equiaxial growth of recrystallized grains, the influence of nearest neighbors is considered by adopting Von-Neumann neighbor type.

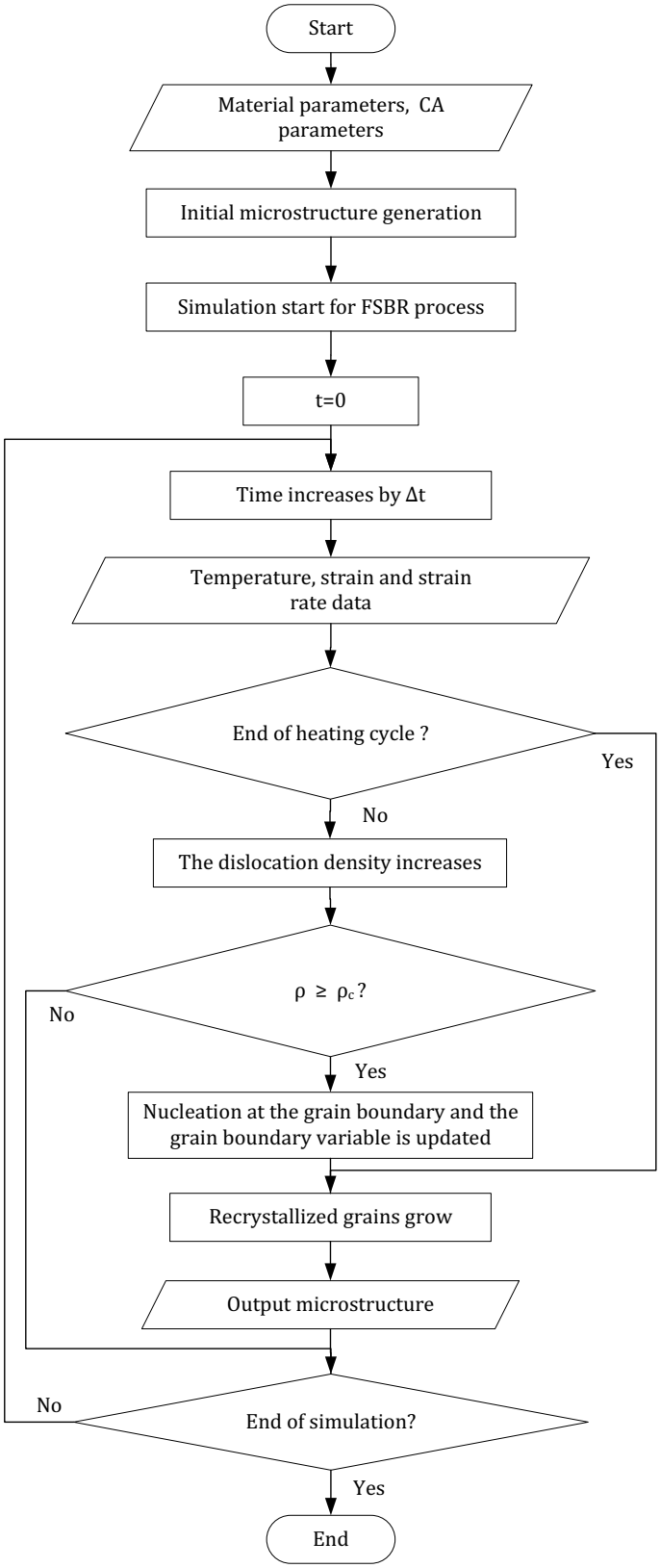

Fig. 4: Flow chart for CA model

5. A running step representative time: According to equation 11 and 12, every simulation step simulates the recrystallization grain boundary mobility. The grain growth driving force is not the same for each step. To achieve a reasonable conversion between each simulation step and the actual deformation time increment, it is important to ensure that at least one cell in the simulation system has undergone an orientation transition where it is moved by one cell length.

In this paper, we take the minimum time required to grow a cell as the actual time Δt corresponding to one step of the model.

$$\Delta t = \frac{L_{\mathrm{CA}}}{V_{\max}} \tag{14}$$

where V_{max} is maximum grain boundary moving rate and L_{CA} is unit cell side length. The expression for Δt can be simplified as follows:

$$\Delta t = \frac{L_{\mathrm{CA}}}{M \Delta F_{\max}} \tag{15}$$

where ΔF_{max} is maximum grain boundary migration driving force. Then the strain increase for a time step can be expressed as

$$\Delta \varepsilon = \dot{\varepsilon} \Delta t = \dot{\varepsilon} \frac{L_{\mathrm{CA}}}{M \Delta F_{\max}} \tag{16}$$

3.6 Dynamic Recrystallization Simulation Flow

The microstructure evolution during FSBR process with dynamic recrystallization. The model is simulated for deformation and heat generation of a single pass of friction stir penetration. The detailed steps for the simulation are as follows:

1. Input the relevant parameters of the material and heat deformation conditions. Enter the initial value, including: gas constant R, activation energy Q_{act}, shear modulus μ, Burgess vector b, temperature (T) history, equivalent strain history, strain rate history.
2. Generate the initial grain distribution is generated using section 3.5. The grain orientation was randomized to a positive integer between 0 and 180, and the cell recrystallization state was set to zero.
3. Dislocation density increases according to dislocation density evolution in section 3.2 for each time step. The average dislocation density at different times is determined by the average of the dislocation densities of all the cells in the region:

$$\bar{\rho} = \frac{1}{NN} \sum_{i,j}^{NN} \rho_{i,j} \tag{17}$$

where $\rho_{i,j}$ is dislocation density at the cell site and NN is the total number of cells in the simulation region.

4. Recrystallization nucleation: the nucleation of recrystallized grain is randomly distributed along the grain boundary during the simulation of CA. For a particular time step, the nucleation probability for a certain cell is given by

$$p_{nuc} = \dot{n} \times \Delta t \times S_{CA} \quad (18)$$

where Δt is the actual time corresponding to a step size and S_{CA} is the area of the unit cell, for square cells, $S_{CA} = L_{CA}^2$, L_{CA} is a single cell length size.

The random number *rand* is inserted into each time step. If *rand* < p_{nuc}, the cell becomes a dynamic recrystallization nucleus. The orientation number of the cell is randomly assigned in the range of 1-180 and the value of the six state variables correspondingly updated. The dislocation density variable is set to its dislocation density was set to a very small number. If rand > p_{nuc}, the cells do not undergo dynamic recrystallization nucleation.

5. Dynamic recrystallization grain growth: The recrystallized grains of newborns continue to grow so that the grain boundary migrates continuously. The migration distance of recrystallized grain boundaries is determined by:

$$L_G = V_i \Delta t \quad (19)$$

During the deformation, the driving force for grain growth of the recrystallized grains will gradually slow down, and the grain stop length will be reduced when the grain boundary is moved by one cell length in a time step. Large or recrystallized grains collide with the cells of other recrystallized grains, the two grains stop growing in the same direction at the same time. The detailed flow chart is shown in Fig. 4.

4. SIMULATION RESULTS AND DISCUSSIONS

It is clearly observable that the material microstructure went through significant evolution during the process at different location away from the hole surface. According to the grain size, hardness, the processed microstructure can be classified in different zones as follows:

Zone A: x < 26 μm away from hole edge
Zone B: 26 μm > x > 88 μm away from hole edge
Zone C: 88 μm > x > 363 μm away from hole edge
Unaffected: x >363μm away from hole edge

Unaffected zone had similar microstructure and average grain size as base material. As we move to Zone C, we see the grains started to reduce in size. The average grain size reduces significantly to 14.3±1.0 μm. This indicates that amount of shear deformation started to increase as we moved to zone C. As we moved more towards hole surface, significantly smaller grains can be observed. As we go into the zone B which is between 88 μm and 26 μm, elongated grains with high aspect ratio can be seen as in Fig. 3a. The grain size is reduced significantly and average grain width reduces to 6.76±0.58 μm. On the contrary, in zone A, those elongated grains are dissolved and finer grains has evolved (Fig. 3b). Average grain size is close to 1μm and some grains were below 1 μm as well.

Simulated microstructural evolution during DRX is done using the material properties of AA6111-T4 as listed in Table 3.

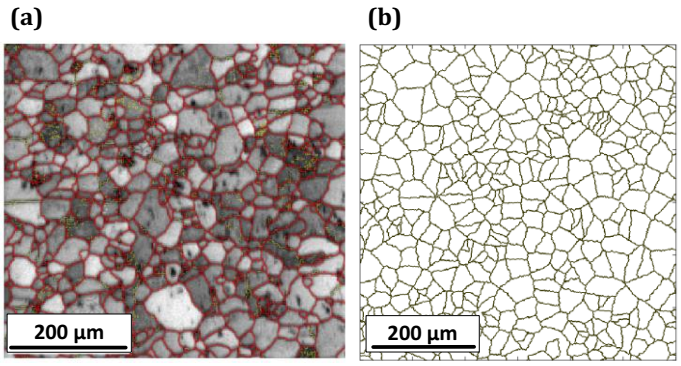

Fig. 5: Initial microstructure comparison : (a) Initial microstructure of the AA6111-T4 by EBSD [27]; (b) Simulated initial microstructure of the AA6111-T4;

Fig. 5 shows the comparison of initial microstructure. EBSD analysis prior to the experiment. The initial mean diameter of the primary grains is 26.5±1.8 μm. This is close to the experimental measurement of 24.9±1.9 μm. Exact match is difficult as the initial microstructure generation algorithm is based on random allocation of nucleation points.

The simulated microstructure evolution of the AA6111-T4 during FSBR process is shown in Fig. 6a-c under thermomechanical condition (temperature and strain rate distribution) across the simulation domain. The right boundary of the domain is physically equivalent to the hole surface. This boundary has higher temperature and strain rate compared to the left boundary which is 400 μm away from the hole surface. As the simulation progresses DRX nucleation starts at the grain boundary near the right side boundary (Fig. 6a) and slowly spread towards left boundary (Fig. 6b) as the simulation progresses.

After the heating cycle is over which means the frictional penetration is finished the material starts cooling. As the bulk material is still at low temperature, the cooling rate is very fast. The DRX nucleation stops immediately at the right boundary. The final grain distribution after the completion of cooling cycle is shown in Fig. 6c.

The Fig. 6d shows the experimental result of DRX completion in right side boundary as this region has high strain rate and high temperature distribution. The simulation result shows that the right boundary has smaller grain size 2.35±0.05 μm as shown in Fig. 6c. It shows that these fine grains are distributed within a distance of ~100 μm away from the hole surface. The size fine grains on the right boundary agrees well with the experimental result (Fig. 6d) by Min et. al. [27] .The experimentally measured size of the fine grain area is 88μm. This error might be attributed from the assigned temperature boundary conditions in the simulation as it is very difficult to capture accurate temperature distribution in such a small resolution experimentally.

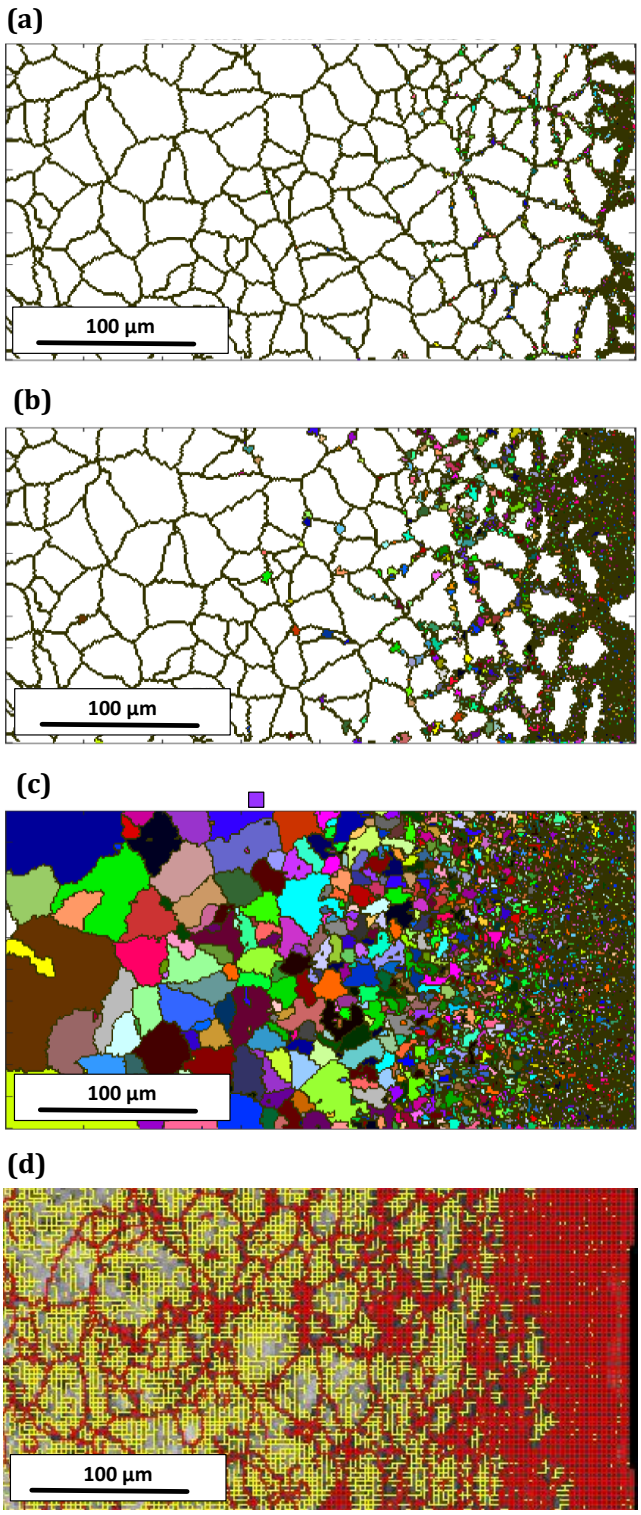

Fig. 6: Evolution of microstructure during CA simulation: (a) DRX nucleation near the right side boundary, (b) DRX nucleation spread towards left boundary; (c) final simulated grain structure; (d) experimental grain structure (experimental images adopted from [27]

Fig. 7 compares the simulated grain distribution across different zones with experimental findings. Our current analysis domain is based on the zone A, B and C as mentioned in section 2. The simulated average grain size agrees well with the experimentally calculated grain sizes.

As a final note, evolution of sub-micron grains is not captured in this model. The resolution of the simulation domain is currently limited to 1µm. As a result, this model is unable to capture the submicron grains near the hole edge. The future goal is to implement gradient resolution across the analysis domain by modifying the model parameters as a function of resolution.

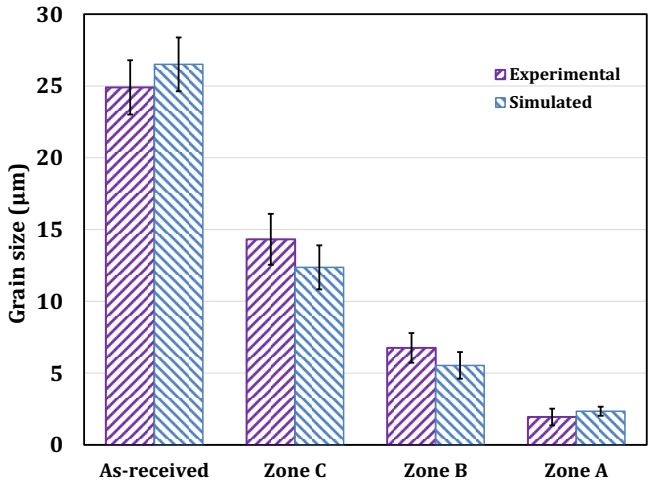

Fig. 7: Simulated grain size comparison

5. CONCLUSIONS

The evolution of microstructure evolution by DRX in friction stir blind riveting process is first time successfully modeled using CA method. A MATLAB code has been developed to implement the CA method to capture the microstructure evolution during the process. The DRX of grains is modeled based on the evolution of dislocation density during the process loading condition in terms of temperature, strain rate and strain distribution across the domain.

The simulated initial grain size distribution agreed well with the experimental EBSD measurement. The simulation result demonstrated that the high temperature and strain rate distribution at the friction stir riveted hole triggered dynamic recrystallization. The final grain size distribution is predicted and validated with experimental measurement. Simulation result agrees well with the experimental EBSD data. In the future work, this CA model will be improved for analysis of sub-micron grains and it will be used to capture the microstructure evolution as a function of different process condition.

ACKNOWLEDGEMENT

The authors gratefully acknowledge the financial support by the National Science Foundation under Grant Number CMMI-1537512 and CMMI 1651024.

REFERENCES

[1] Wang, P.-C., and Stevenson, R., 2006, "Friction stir rivet method of joining," United States Patent and Trade Office, **US7862271**.

[2] Gao, D., Ersoy, U., Stevenson, R., and Wang, P., 2009, "A New One-Sided Joining Process for Aluminum Alloys : Friction Stir," Journal of Manufacturing Science and Engineering, **131**, pp. 1–12.

[3] Lathabai, S., Tyagi, V., Ritchie, D., Kearney, T., Finnin, B., Christian, S., Sansome, A., and White, G., 2011, "Friction Stir Blind Riveting: A Novel Joining Process for Automotive Light Alloys," SAE International Journal of Materials and Manufacturing, **4**(1), pp. 589–601.

[4] Min, J., Li, J., Li, Y., Carlson, B. E., Lin, J., and Wang, W., 2015, "Friction stir blind riveting for aluminum alloy sheets," Journal of Materials Processing Tech., **215**, pp. 20–29.

[5] Min, J., Li, J., Carlson, B. E., Li, Y., Quinn, J. F., Lin, J., and Wang, W., 2015, "Friction Stir Blind Riveting for Joining Dissimilar Cast Mg AM60 and Al Alloy Sheets," ASME Journal of Manufacturing Science and Engineering, **137**(5), p. 51022.

[6] Min, J., Li, Y., Carlson, B. E., Hu, S. J., Li, J., and Lin, J., 2015, "A new single-sided blind riveting method for joining dissimilar materials," CIRP Annals - Manufacturing Technology, **64**(1), pp. 13–16.

[7] Min, J., Li, Y., Li, J., Carlson, B. E., and Lin, J., 2015, "Friction stir blind riveting of carbon fiber-reinforced polymer composite and aluminum alloy sheets," The International Journal of Advanced Manufacturing Technology, **76**(5–8), pp. 1403–1410.

[8] Zheng, C., Xiao, N., Li, D., and Li, Y., 2008, "Microstructure prediction of the austenite recrystallization during multi-pass steel strip hot rolling: A cellular automaton modeling," Computational Materials Science, **44**(2), pp. 507–514.

[9] Yazdipour, N., Davies, C. H. J., and Hodgson, P. D., 2008, "Microstructural modeling of dynamic recrystallization using irregular cellular automata," Computational Materials Science, **44**(2), pp. 566–576.

[10] Jin, Z., and Cui, Z., 2010, "Investigation on strain dependence of dynamic recrystallization behavior using an inverse analysis method," Materials Science and Engineering: A, **527**(13–14), pp. 3111–3119.

[11] Jin, Z., and Cui, Z., 2012, "Investigation on dynamic recrystallization using a modified cellular automaton," Computational Materials Science, **63**, pp. 249–255.

[12] Chen, F., Cui, Z., Liu, J., Zhang, X., and Chen, W., 2009, "Modeling and simulation on dynamic recrystallization of 30Cr2Ni4MoV rotor steel using the cellular automaton method," Modelling and Simulation in Materials Science and Engineering, **17**(7), p. 75015.

[13] Chen, F., Cui, Z., Liu, J., Chen, W., and Chen, S., 2010, "Mesoscale simulation of the high-temperature austenitizing and dynamic recrystallization by coupling a cellular automaton with a topology deformation technique," Materials Science and Engineering: A, **527**(21–22), pp. 5539–5549.

[14] Chen, F., and Cui, Z., 2012, "Mesoscale simulation of microstructure evolution during multi-stage hot forging processes," Modelling and Simulation in Materials Science and Engineering, **20**(4), p. 45008.

[15] Chen, F., Qi, K., Cui, Z., and Lai, X., 2014, "Modeling the dynamic recrystallization in austenitic stainless steel using cellular automaton method," Computational Materials Science, **83**, pp. 331–340.

[16] Hallberg, H., Wallin, M., and Ristinmaa, M., 2010, "Simulation of discontinuous dynamic recrystallization in pure Cu using a probabilistic cellular automaton," Computational Materials Science, **49**(1), pp. 25–34.

[17] GOETZ, R., 2005, "Particle stimulated nucleation during dynamic recrystallization using a cellular automata model," Scripta Materialia, **52**(9), pp. 851–856.

[18] Qian, M., and Guo, Z. ., 2004, "Cellular automata simulation of microstructural evolution during dynamic recrystallization of an HY-100 steel," Materials Science and Engineering: A, **365**(1–2), pp. 180–185.

[19] Kugler, G., and Turk, R., 2004, "Modeling the dynamic recrystallization under multi-stage hot deformation," Acta Materialia, **52**(15), pp. 4659–4668.

[20] Xiao, N., Zheng, C., Li, D., and Li, Y., 2008, "A simulation of dynamic recrystallization by coupling a cellular automaton method with a topology deformation technique," Computational Materials Science, **41**(3), pp. 366–374.

[21] Ding, R., and Guo, Z. ., 2001, "Coupled quantitative simulation of microstructural evolution and plastic flow during dynamic recrystallization," Acta Materialia, **49**(16), pp. 3163–3175.

[22] Ding, H., Liu, L., Kamado, S., Ding, W., and Kojima, Y., 2009, "Investigation of the hot compression behavior of the Mg–9Al–1Zn alloy using EBSP analysis and a cellular automata simulation," Modelling and Simulation in Materials Science and Engineering, **17**(2), p. 25009.

[23] Liu, X., Li, L., He, F., Zhou, J., Zhu, B., and Zhang, L., 2013, "Simulation on dynamic recrystallization behavior of AZ31 magnesium alloy using cellular automaton method coupling Laasraoui–Jonas model," Transactions of Nonferrous Metals Society of China, **23**(9), pp. 2692–

2699.

[24] Yin, H., and Felicelli, S. D., 2009, "A cellular automaton model for dendrite growth in magnesium alloy AZ91," Modelling and Simulation in Materials Science and Engineering, **17**(7), p. 75011.

[25] Wu, C., Yang, H., and Li, H., 2013, "Modeling of static coarsening of two-phase titanium alloy in the α+β two-phase region at different temperature by a cellular automata method," Chinese Science Bulletin, **58**(24), pp. 3023–3032.

[26] Zhang, Y., Jiang, S., Liang, Y., and Hu, L., 2013, "Simulation of dynamic recrystallization of NiTi shape memory alloy during hot compression deformation based on cellular automaton," Computational Materials Science, **71**, pp. 124–134.

[27] Min, J., Li, J., Li, Y., Carlson, B. E., and Lin, J., 2016, "Affected Zones in an Aluminum Alloy Frictionally Penetrated by a Blind Rivet," Journal of Manufacturing Science and Engineering, **138**, pp. 1–6.

[28] Agarwal, S., Briant, C. L., Hector, L. G., and Chen, Y. L., 2007, "Friction stir processed AA5182-O and AA6111-T4 aluminum alloys. Part 1: Electron backscattered diffraction analysis," Journal of Materials Engineering and Performance, **16**(4), pp. 391–403.

[29] Özel, T., and Zeren, E., 2005, "Finite element method simulation of machining of AISI 1045 steel with a round edge cutting tool," Proceedings of the 8th CIRP International.

[30] Mishra, R. S., and Ma, Z. Y., 2005, "Friction stir welding and processing," Materials Science and Engineering: R: Reports, **50**(1–2), pp. 1–78.

[31] Ding, H., and Shin, Y. C., 2014, "Dislocation Density-Based Grain Refinement Modeling of Orthogonal Cutting of Titanium," ASME Journal of Manufacturing Science and Engineering, **136**(4), p. 41003.

[32] Ding, H., Shen, N., and Shin, Y. C., 2012, "Predictive modeling of grain refinement during multi-pass cold rolling," Journal of Materials Processing Technology, **212**(5), pp. 1003–1013.

[33] Shen, N., Samanta, A., Ding, H., and Cai, W. W., 2016, "Simulating microstructure evolution of battery tabs during ultrasonic welding," SME Journal of Manufacturing Processes, **23**, pp. 306–314.

[34] Sellars, C. M., and Whiteman, J. A., 1979, "Recrystallization and grain growth in hot rolling," Metal Science, **13**(3–4), pp. 187–194.

[35] Peczak, P., 1995, "A Monte Carlo study of influence of deformation temperature on dynamic recrystallization," Acta Metallurgica et Materialia, **43**(3), pp. 1279–1291.

[36] Hordon, M. ., and Averbach, B. ., 1961, "X-ray measurements of dislocation density in deformed Copper and Aluminum single crystals," Acta Metallurgica, **9**(3), pp. 237–246.

[37] Williamson, G. K., and Smallman, R. E., 1955, "III. Dislocation densities in some annealed and cold-worked metals from measurements on the X-ray debye-scherrer spectrum," Philosophical Magazine, **1**(1), pp. 34–46.

[38] McQueen, H. J., 1988, "Initiating nucleation of dynamic recrystallization, primarily in polycrystals," Materials Science and Engineering: A, **101**(0), pp. 149–160.

[39] Sakai, T., Akben, M. G., and Jonas, J. J., 1983, "Dynamic recrystallization during the transient deformation of a vanadium microalloyed steel," Acta Metallurgica, **31**(4), pp. 631–641.

[40] Mecking, H., and Kocks, U. F., 1981, "Kinetics of flow and strain-hardening," Acta Metallurgica, **29**(11), pp. 1865–1875.

[41] Mecking, H., 1981, "Strain hardening and dynamic recovery," Dislocation Modelling of Physical Systems, M.F. Ashby, R. Bullough, C.S. Hartley, and J.P. Hirth, eds., Pergamon, pp. 197–211.

[42] Estrin, Y., 1996, "2 - Dislocation Density Related Constitutive Modeling," Unified Constitutive Laws of Plastic Deformation, A.S. Krausz, and K. Krausz, eds., Academic Press, San Diego, pp. 69–106.

[43] Stüwe, H. P., and Ortner, B., 1974, "Recrystallization in Hot Working and Creep," Metal Science, **8**(1), pp. 161–167.

[44] Roberts, W., and Ahlblom, B., 1978, "A nucleation criterion for dynamic recrystallization during hot working," Acta Metallurgica, **26**, pp. 801–813.

[45] Ding, H., Shen, N., and Shin, Y. C., 2011, "Modeling of grain refinement in aluminum and copper subjected to cutting," Computational Materials Science, **50**(10), pp. 3016–3025.

[46] Frost, H. J., and Ashby, F., 1982, Deformation-mechanism maps: the plasticity and creep of metals and ceramics, Pergamon Press, Kidlington, Oxford, United Kingdom.

[47] Peczak, P., and Luton, M. J., 1993, "A Monte Carlo study of the influence of dynamic recovery on dynamic recrystallization," Acta Metallurgica et Materialia, **41**(1), pp. 59–71.